Contribution from the Department of Chemistry,
The University of North Carolina, Chapel Hill, North Carolina 27514

Electronic Structure and Redox Properties of the Clusters $[Ru_3O(CH_3CO_2)_6L_3]^{n+}$

JOHN A. BAUMANN, DENNIS J. SALMON, STEPHEN T. WILSON, THOMAS J. MEYER,*
and WILLIAM E. HATFIELD

Received March 1, 1978

A series of oxo-bridged, triruthenium cluster complexes, $[Ru_3O(CH_3CO_2)_6(py)_2L]^+$ (L = pyridine, pyrazine (pyr), 4,4′-bipyridine (4,4′-bpy), *trans*-1,2-bis(4-pyridyl)ethylene (BPE), and 1,2-bis(4-pyridyl)ethane (BPA), have been prepared as PF_6^- salts. Electrochemical studies show that the clusters can exist in a series of redox states, $[Ru_3O(CH_3CO_2)_6L_3]^n$ (n = +3, +2, +1, 0, −1, −2). Clusters in the +2 and 0 states have been isolated following chemical or electrochemical oxidation or reduction of the +1 clusters. The effects of changes in electron content on the chemical and physical properties of the clusters have been investigated by spectral, magnetic resonance, and electrochemical measurements. The +2, +1, and 0 clusters all absorb light strongly in the visible region because of a series of closely spaced resolvable electronic transitions. All three clusters, including the mixed-valence +2 (Ru(III)–Ru(III)–Ru(IV) in a localized valence description) and 0 (Ru(II)–Ru(III)–Ru(III)) clusters, have a single Ru $3d_{5/2}$ binding energy by ESCA and the shifts in binding energies with changes in the electron content of the clusters are small. The electronic properties of all three clusters can be interpreted in terms of a qualitative molecular orbital scheme which assumes strong Ru–Ru interactions through the central oxide ion and metal–metal interactions by direct metal–metal bonding. Using the scheme, the origins of both the multiple oxidation state and spectral properties of the clusters lie in a series of delocalized Ru–Ru and Ru–O–Ru levels based on the Ru_3O core. Compared to related clusters, the carbonyl cluster $[Ru_3O(CH_3CO_2)_6(py)_2(CO)]$ has its own distinct chemical and physical properties apparently because of strong, localized back-bonding from Ru to CO at the single Ru–CO site in the cluster.

Introduction

The μ-oxo, carboxylate-bridged cluster unit found, for example, in $[Ru_3O(CH_3CO_2)_6(py)_3]$ (py is pyridine) is remarkably common in transition-metal chemistry. Examples of such clusters are known for a series of M(III) ions where M is Cr, Mn, Fe, Co, Rh, Ir, and Ru. Spencer and Wilkinson[1] have investigated the chemistry of the ruthenium clusters in detail. Their work has included the preparation of a series of clusters in which both the bridging carboxylates and the terminal ligands L (Figure 1) have been varied systematically. Spencer and Wilkinson also studied the redox properties of the clusters chemically and electrochemically and described their optical spectra and magnetic properties. The crystal structure of the mixed-valence cluster $[Ru_3O(OAc)_6(PPh_3)_3]$ has been determined by Cotton and Norman,[2] and as shown in Figure 1, consists of a planar triangular array of equivalent ruthenium sites which share a tribridging oxo ligand.

Our interest in the ruthenium clusters comes from two themes in our current work. One concerns the preparations and properties of mixed-valence compounds.[3-6] Earlier work on dimeric systems like $[(bpy)_2ClRuORuCl(bpy)_2]^{3+/2+/+}$[7] and $[(bpy)_2ClRu(pyr)RuCl(bpy)_2]^{3+}$[8,9] has shed light on the factors which determine whether valences are localized or delocalized in mixed-valence dimers. This work has also given insight into optical and thermal intramolecular electron-transfer processes in dimers where there are localized valences.[4,8,9] The ruthenium clusters are of interest in this context because they have an extensive, reversible redox chemistry and therefore an extensive mixed-valence chemistry. In addition, given the basic structural details of the cluster and the synthetic chemistry available, the cluster unit is potentially capable of acting as a building block for the preparation of ligand-bridged, mixed-valence oligomers.

In addition to our interest in their mixed-valence properties, the clusters are promising as potential homogeneous redox catalysts. They are stable in a series of different redox states offering the possibility of multiple electron-transfer steps and have binding sites on the periphery for holding substrate molecules.

Part of the work described here has appeared as a preliminary communication.[10]

Experimental Section

Measurements. Ultraviolet, visible, and near-infrared spectra were recorded using Cary Models 14 and 17 and Bausch and Lomb Model 210 spectrophotometers. Spectral deconvolution was accomplished using the program SPECSOLV,[11] a local variation of the program BIGAUS.[12]

Infrared spectra were recorded on a Perkin-Elmer 421 spectrophotometer in KBr pellets, at room temperature. Electrochemical measurements made were vs. the saturated sodium calomel electrode (SSCE) at 22 ± 2 °C and are uncorrected for junction potential effects. The measurements were made using a PAR Model 173 potentiostat for potential control with a PAR Model 175 universal programmer as a sweep generator for voltammetric experiments. Electrochemical reversibility was determined by cyclic voltammetry, based on the ratio of cathodic to anodic peak currents ($i_{p,c}/i_{p,a}$ = 1) and the potential separation of the peaks (ΔE_p). All voltammetric measurements were carried out at platinum electrodes in solutions, deaerated by a stream of dry argon when necessary.

Materials. Tetra-*n*-butylammonium hexafluorophosphate (TBAH) was prepared by standard techniques, recrystallized three times from hot ethanol–water mixtures, and vacuum dried at 70 °C for 10 h. Acetonitrile (MCB Spectrograde) was dried over Davison 4-Å molecular sieves for electrochemical measurements and used without drying for spectral measurements. Water was deionized and then distilled from alkaline permanganate. All other solvents (reagent grade) were used without further purification. The ligands, pyrazine (pyr), 4,4′-bipyridine (4,4′-bpy), *trans*-1,2-bis(4-pyridyl)ethylene (BPE), and 1,2-bis(4-pyridyl)ethane (BPA), were obtained commercially and used without further purification. Argon was purified by passing it through a heated column of activated Catalyst R3-11 (Chemical Dynamics Corp.) and then through drying tubes containing Drierite. Elemental analyses were carried out by Galbraith Laboratories, Knoxville, Tenn., PCR, Inc., Gainesville, Fla., and Integral Microanalytical Laboratories, Raleigh, N.C.

Preparations. $[Ru_3O(OAc)_6(CH_3OH)_3]^+$ (1) (OAc = CH_3CO_2). This ion was used as the starting material for all subsequent preparations and a stock solution was generated by modifying the method of Spencer and Wilkinson.[1a] $RuCl_3 \cdot 3H_2O$ (3.0 g, 12 mmol) and sodium acetate (6.0 g, 44 mmol) were placed in a 300-mL round-bottom flask. A 75-mL aliquot of absolute ethanol and 75 mL of glacial acetic acid were added. After being heated at reflux for 4 h or more, the solution was cooled. Several methods were available to separate the product from excess salts. The most efficient was to centrifuge the mixture for about 20 min at a medium speed and filter the resulting supernatant liquid. The filtrate was reduced to a green oil by removing the volatiles on a rotary evaporator. A total of 150 mL of CH_3OH was added to the oil and the solution was stirred and then filtered. Again, the volatiles were removed from the filtrate by evaporation. Dissolution of the resultant oil in 100 mL of CH_3OH gave a solution approximately 0.04 M in $Ru_3O(OAc)_6(CH_3OH)_3^+$. Though probably impure, the solution was suitable for subsequent reactions. The preparations of the next four complexes, $[Ru_3O(OAc)_6(py)_3](PF_6)$, $[Ru_3O(OAc)_6(py)_3]$, $[Ru_3O(OAc)_6(CO)(py)_2] \cdot C_6H_6$, and $[Ru_3O(OAc)_6(py)_2(CH_3OH)](PF_6)$, are also

0020-1669/78/1317-3342$01.00/0

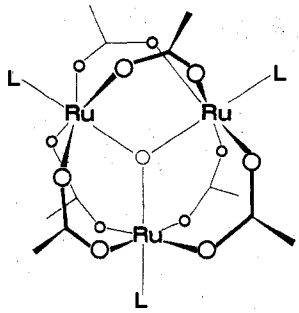

Figure 1. Structure of the cluster unit $[Ru_3O(CH_3CO_2)_6(L)_3]$.[2]

modifications of the general procedures given by Spencer and Wilkinson.[1]

$[Ru_3O(OAc)_6(py)_3](PF_6)$ (2). Twenty-five milliliters of a stock solution of **1** was diluted with methanol to 50 mL, 3 mL of pyridine was added, and the solution was heated at reflux for 5 min. Heating was discontinued and a solution of 0.5 g of NH_4PF_6 in a minimum of methanol was added slowly to the solution containing the complex. When all the NH_4PF_6 had been added and the resulting mixture cooled to room temperature, a blue solid was collected by filtration. The solid was washed thoroughly with water and then with 3 × 3 mL of methanol and air-dried; yield 640 mg (60% based on starting Ru). Anal. Calcd for $C_{27}H_{33}N_3O_{13}Ru_3PF_6$: C, 30.72; H, 3.15; N, 3.98. Found: C, 30.73; H, 2.78; N, 3.95.

$[Ru_3O(OAc)_6(py)_3]$ (3). Twenty-five milliliters of a stock solution of **1** was diluted to 50 mL with methanol. Pyridine (3 mL) was added and the solution was heated at reflux for 5 min. The solution was cooled to 0 °C in an ice bath and hydrazine (65% in H_2O) was added dropwise with stirring until a green solid became visible as a suspension. The mixture was stirred for 15 min and 1–2 additional drops of hydrazine were added. The green solid was filtered off and washed thoroughly with water, with methanol, and finally copiously with ethyl ether (Et_2O). Following brief air drying, the solid was dried in vacuo. Anal. Calcd for $C_{27}H_{33}N_3O_{13}Ru_3$: C, 35.61; H, 3.65; N, 4.61. Found: C, 35.20; H, 3.74; N, 4.32.

$[Ru_3O(OAc)_6(CO)(py)_2]\cdot C_6H_6$ (4). To a nitrogen- or argon-saturated solution of 75 mL of benzene and 25 mL of methanol was added 1 g of $Ru_3O(OAc)_6(py)_3$. The solution was heated at reflux under a gentle flow of CO for 5 h. The resulting blue solution was cooled and filtered. The dark blue lustrous solid which was collected was washed with Et_2O and air-dried; yield 650 mg (65% of theory). Anal. Calcd for $C_{29}H_{34}N_2O_{14}Ru_3$: C, 37.14; H, 3.65; N, 2.99. Found: C, 36.90; H, 3.36; N, 3.01.

$[Ru_3O(OAc)_6(py)_2(CH_3OH)](PF_6)$ (5). A portion of the bis(pyridine)carbonyl complex $Ru_3O(OAc)_6(CO)(py)_2\cdot C_6H_6$ (500 mg, 0.53 mmol) was dissolved in 50 mL of dichloromethane. Ten milliliters of 0.15 M Br_2 in CH_2Cl_2 (threefold excess) was added. The resulting solution was stirred for 10 min and volatiles were removed at reduced pressure. A suspension of the residue in 40 mL of methanol was heated at reflux until a homogeneous blue solution was observed. The solution was allowed to cool slowly and a solution of NH_4PF_6 (0.5 g, 3 mmol) in a minimum of methanol was added slowly. The resulting solution was cooled to 0 °C and filtered. A light blue solid was collected, washed with CH_3OH (2 × 2 mL) and ether, and then air-dried; yield 365 mg (62% of theory). Anal. Calcd for $C_{23}H_{32}N_2O_{14}Ru_3PF_6$: C, 27.39; H, 3.20; N, 2.78. Found: C, 27.30; H, 3.17; N, 2.88.

$[Ru_3O(OAc)_6(py)_2L](PF_6)$ (6) (L = pyr, 4,4′-bpy, BPE, or BPA). In a typical preparation, the bis(pyridine)methanol complex $[Ru_3O(OAc)_6(py)_2(CH_3OH)](PF_6)$ (208.48 mg, 0.27 mmol) was allowed to react with excess pyrazine (203.00 mg, 2.872 mmol) in methylene chloride at room temperature (ca. 25 mL) for 18 h or more. After 18 h, the solution was filtered into stirring ethyl ether which precipitated the salt $[Ru_3O(OAc)_6(py)_2pyr](PF_6)$ (**6a**). The product was collected by suction filtration, washed with ether, air-dried, and then vacuum dried (205 mg, 94% yield). The 4,4′-bpy and BPE complexes (**6b** and **6c**, respectively) were prepared in the same fashion, but recrystallized by dissolving in CH_2Cl_2 and slowly adding petroleum ether (bp 60–90 °C) dropwise to the stirred solution until crystallization occurred. After collection and air drying of the crystals, yields of 92 and 93.5% were obtained, respectively. The BPA complex, **6d**, was obtained in an analogous manner, but the CH_2Cl_2/Et_2O precipitation step was eliminated and the solid obtained directly by the addition of petroleum ether to the dichloromethane solution giving a 98% yield. Anal. Calcd for **6a**, $C_{26}H_{32}N_4O_{13}Ru_3PF_6$: C, 29.55; H, 3.05; N, 5.30. Found: C, 29.80; H, 3.13; N, 5.42. Calcd for **6b**, $C_{32}H_{36}N_4O_{13}Ru_3PF_6$: C, 33.93; H, 3.20; N, 4.95. Found: C, 33.80; H, 3.06; N, 4.70. Calcd for **6c**, $C_{34}H_{38}N_4O_{13}Ru_3PF_6$: C, 35.24; H, 3.31; N, 4.84. Found: C, 35.15; H, 3.20; N, 4.70. Calcd for **6d**, $C_{34}H_{40}N_4O_{13}Ru_3PF_6$: C, 35.18; H, 3.47; N, 4.83. Found: C, 35.24; H, 3.50; N, 4.94.

$[Ru_3O(OAc)_6(py)_2pyr]$ (7). The +1 ion $[Ru_3O(OAc)_6(py)_2pyr]^+$ was reduced to the neutral complex by suspending 100 mg of the PF_6^- salt in 25 mL of methanol. A few drops of dilute (5–10%) aqueous hydrazine were added with stirring. After a golden brown color appeared in the solution, 25 mL of H_2O was added and the methanol was removed on a rotary evaporator, without heating. A brown solid crystallized from solution and was collected, washed extensively with water, and vacuum dried. Anal. Calcd for $C_{26}H_{32}N_4O_{13}Ru_3$: C, 34.25; H, 2.55; N, 6.14. Found: C, 33.63; H, 3.18; N, 6.02.

$[Ru_3O(OAc)_6(py)_3](PF_6)_2$ (8a), $[Ru_3O(OAc)_6(py)_2pyr](PF_6)_2$ (8b). The dications $[Ru_3O(OAc)_6(py)_3]^{2+}$ and $[Ru_3O(OAc)_6(py)_2pyr]^{2+}$ were prepared by dissolving the appropriate starting +1 clusters in minimum amounts of 0.1 M $TBAH/CH_2Cl_2$ and oxidizing electrochemically with a Pt gauze electrode at 1.2 V vs. the SSCE until the current had fallen to near zero. The complexes, which precipitated from solution as PF_6^- salts, were collected by suction filtration, washed with CH_2Cl_2, air-dried, and vacuum dried. Anal. Calcd for **8a**, $C_{27}H_{33}N_3O_{13}Ru_3P_2F_{12}$: C, 27.01; H, 2.77; N, 3.50. Found: C, 26.89; H, 2.63; N, 3.46. Calcd for **8b**, $C_{26}H_{32}N_4O_{13}Ru_3P_2F_{12}$: C, 25.99; H, 2.68; N, 4.66. Found: C, 25.79; H, 3.02; N, 4.67.

$[Ru_3O(OAc)_6(2\text{-}Me(pyr))_3]$ (9) (2-Me(pyr) = 2-Methylpyrazine). An excess (1.5 mL) of 2-methylpyrazine was added to 10 mmol of $[Ru_3O(OAc)_6(CH_3OH)_3](OAc)$ in 25 mL of methanol. The resulting solution was heated at reflux for 12 h at 45 °C under a stream of N_2. After cooling of the mixture, a brown solid was collected by filtration and washed well with water, with 3 × 2 mL of methanol, and finally with small portions of ether. The resulting solid was then air-dried and dried under vacuum. Anal. Calcd for $C_{27}H_{34}N_4O_{13}Ru_3$: C, 33.93; H, 3.80; N, 8.80. Found: C, 33.97; H, 3.73; N, 7.70.

$[Ru_3O(OAc)_6(2\text{-}Me(pyr))_3](PF_6)$ (10). The neutral 2-methylpyrazine cluster **9** was oxidized to the +1 cluster by dissolving the complex in CH_2Cl_2 and adding excess bromine in CH_2Cl_2. The two solutions were mixed and allowed to stand for 15 min. The resulting solution was stripped of volatiles on a rotary evaporator. The residue was dissolved in a minimum of methanol and the solution heated at reflux for 10 min. While the solution was allowed to cool with stirring, a fivefold excess of NH_4PF_6 dissolved in methanol was added dropwise. After complete addition of the NH_4PF_6 and cooling of the solution to room temperature, the resulting precipitate was filtered off, washed with methanol and then Et_2O, and air-dried. Anal. Calcd for $C_{27}H_{34}N_4O_{13}Ru_3PF_6$: C, 29.46; H, 3.30; N, 7.63. Found: C, 28.91; H, 3.29; N, 7.73.

Results

Syntheses. The solvent complexes $[Ru_3O(OAc)_6(S)_3]^+$ (S = H_2O or CH_3OH) are readily isolable and can be stored for long periods which makes them valuable synthetic intermediates. The solvent molecules, which occupy the terminal cluster coordination sites, are weakly bound and easily displaced by a variety of ligands which allowed Spencer and Wilkinson to prepare a series of symmetrically substituted clusters of the type $Ru_3O(OAc)_6L_3^+$.

Our major synthetic goal here was to develop a route which would allow for sequential substitution at the terminal sites of the cluster. Access to such a route would allow for the preparation of unsymmetrically substituted clusters and, of more importance, to the controlled preparation of dimeric and oligomeric materials where cluster units are linked by bridging ligands.

Reduction of the +1 cluster $[Ru_3O(OAc)_6(py)_3]^+$ using hydrazine as reductant gives the neutral cluster $[Ru_3O(OAc)_6(py)_3]$, and when followed by treatment with CO at room temperature, a single pyridine is displaced giving $[Ru_3O(OAc)_6(CO)(py)_2]$. The carbonyl cluster can be oxidized electrochemically (n = 1 by coulometry) or chemically using Br_2 in CH_2Cl_2 which is more convenient synthetically.

Scheme I

$$[Ru_3O(OAc)_6(py)_3]^+ \xrightarrow{N_2H_4} [Ru_3O(OAc)_6(py)_3] \xrightarrow{CO}$$
$$[Ru_3O(OAc)_6(CO)(py)_2] \xrightarrow{-e^-} [Ru_3O(OAc)_6(CO)(py)_2]^+ \xrightarrow{S}$$
$$[Ru_3O(OAc)_6(S)(py)_2]^+ \xrightarrow{+CH_3OH}$$
$$[Ru_3O(OAc)_6(CH_3OH(py)_2]^+ \xrightarrow{+L'} [Ru_3O(OAc)_6(L')(py)_2]^+$$

S is solvent

The chemical oxidation was shown to be stoichiometric by a spectrophotometric titration. Oxidation is rapid and is followed by loss of CO as observed earlier by Spencer and Wilkinson. The loss of CO from $[Ru_3O(OAc)_6(CO)(py)_2]^+$ is slow on the cyclic voltammetry time scale (seconds) as shown by the electrochemical reversibility of the $[Ru_3O(OAc)_6(CO)(py)_2]^{+/0}$ couple and appears to be complete within a few minutes in CH_2Cl_2 at room temperature. Electrochemical results are discussed in a later section.

Following oxidation of $[Ru_3(OAc)_6(CO)(py)_2]$ to the 1+ ion in acetonitrile, the acetonitrile complex $[Ru_3O(OAc)_6(CH_3CN)(py)_2]^+$ can be isolated and we assume that in dichloromethane solution the vacant coordination site is also occupied by a solvent molecule.

Following oxidation, loss of CO, and evaporation, addition of methanol gives the monomethanol cluster $[Ru_3O(OAc)_6(CH_3OH)(py)_2]^+$. This ion has been isolated and used as a synthetic intermediate in the preparations of the series of unsymmetrically substituted clusters $[Ru_3O(OAc)_6(py)_2L]^+$ (L = pyrazine (pyr), 4,4′-bipyridine (4,4′-bpy), *trans*-1,2-bis(4-pyridyl)ethylene (BPE), or 1,2-bis(4-pyridyl)ethane (BPA). The methanol group is weakly bound and addition

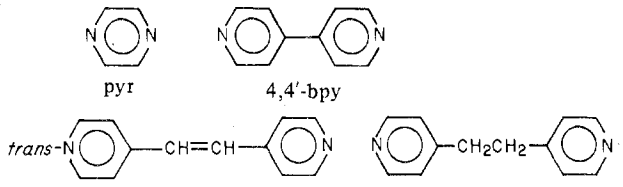

of excess L under mild conditions results in the selective displacement of methanol. In synthetic applications, it has proven more convenient to isolate the methanol complex and use it in a subsequent step rather than to add the ligand L to solutions of the carbonyl cluster which have been oxidized by Br_2. In the latter approach complications can appear, apparently because of competitive substitution reactions involving bromide ion.

The overall reaction scheme used in the preparations is shown in Scheme I. Using similar schemes, we have been able to prepare a series of dimeric and oligomeric, ligand-bridged cluster systems. An initial report on this work has appeared,[10] and further details of the preparations and properties of these interesting materials will appear in subsequent publications.

Oxidation-State Properties. From the results of cyclic voltammetry experiments, Spencer and Wilkinson reported that in aprotic solvents clusters like $[Ru_3O(OAc)_6(py)_3]^+$ undergo a reversible one-electron reduction showing the existence of the reversible couple $[Ru_3O(OAc)_6(py)_3]^{+/0}$. The reversible reduction was reported to be followed by a second one-electron reduction which was irreversible.[1a] We have extended their work on the redox properties of these cluster systems using cyclic voltammetry in acetonitrile. A more or less typical cyclic voltammogram, in this case of the ion $[Ru_3O(OAc)_6(py)_2BPE]^+$, is shown in Figure 2. Electrochemical results obtained for a series of clusters are summarized in Table I. From Figure 2 and the data in Table I, it is evident that the clusters have an extensive reversible electron-transfer chemistry and that, under our conditions, the accessible redox states of the system are $[Ru_3O(OAc)_6(L)_3]^{3+/2+/+/0/1-/2-}$. The $E_{1/2}$ values in Table I were calculated from the averages of anodic and cathodic peak potentials for a given wave ($E_{1/2} = (E_{p,a} + E_{p,c})/2$). The observed peak splittings, $\Delta E_p = E_{p,a} - E_{p,c}$, for the waves were nearly all in the range 60–80 mV independent of sweep rate from 100 to 500 mV/s. The values are slightly larger than the theoretical value of 58 mV, possibly because of uncompensated solution resistance.

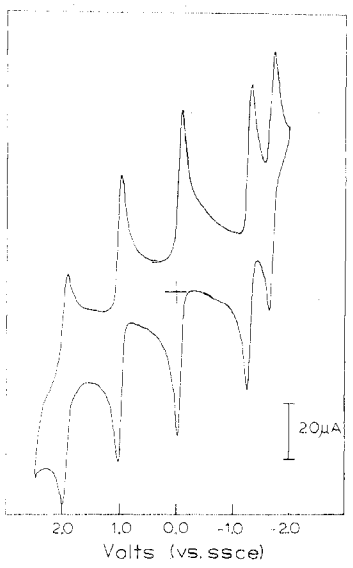

Figure 2. Cyclic voltammogram of $[Ru_3O(OAc)_6(py)_2BPE]^+$ at room temperature in 0.1 M TBAH–CH_3CN at a scan rate of 500 mV/s.

Table I. Electrochemical Data for the Clusters $[Ru_3O(CH_3CO_2)_6(py)_2L]$ and $[Ru_3O(CH_3CO_2)_6L_3]$ in 0.1 M $[N(n\text{-}C_4H_9)_4](PF_6)$–$CH_3CN$ at 22 ± 2 °C

$[Ru_3O(CH_3CO_2)_6(py)_2L]$					
	$E_{1/2}$,[a] V				
L	1 (3+/2+)	2 (2+/1+)	3 (1+/0)	4 (0/1−)	5 (1−/2−)
CH_3OH		1.00	−0.16		
BPA	1.95	1.00	−0.06	−1.34	
BPE	1.96	0.99	−0.05	−1.28	−1.67
4,4′-bpy	1.98	1.00	−0.06	−1.29	−1.83
pyr	2.03	1.04	0.00	−1.20	−1.88
CO		1.26	0.62	−0.88	
$[Ru_3O(CH_3CO_2)_6(L)_3]$					
	$E_{1/2}$,[a] V				
L	1 (3+/2+)	2 (2+/1+)	3 (1+/0)	4 (0/1−)	5 (1−/2−)
py	1.93	0.97	−0.05	−1.32	
2-Me(pyr)	2.08	1.11	+0.10	−1.03	−1.48

[a] $E_{1/2}$ in volts vs. the saturated sodium chloride calomel electrode.

Except for the usually slight correction for differences in diffusion coefficients, the $E_{1/2}$ values are formal reduction potentials for the various redox couples all of which are chemically and electrochemically reversible on the cyclic voltammetry time scale. The reversible couples observed include $[Ru_3O(OAc)_6(L)_3]^{3+/2+}$, $[Ru_3O(OAc)_6(L)_3]^{2+/+}$, $[Ru_3O(OAc)_6(L)_3]^{0/-}$, and $[Ru_3O(OAc)_6(L)_3]^{-/2-}$ in addition to the reversible $[Ru_3O(OAc)_6(L)_3]^{+/0}$ couple observed by Spencer and Wilkinson. The electrochemical experiments reported by Spencer and Wilkinson were carried out in acetone at Pt or Hg electrodes. Their anodic potential sweeps were

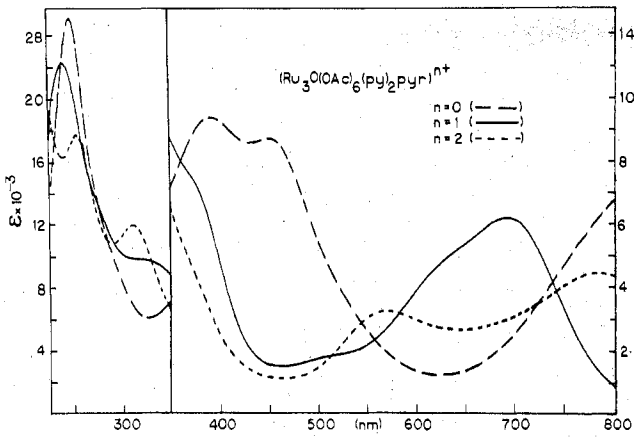

Figure 3. UV–visible absorption spectra of $[Ru_3O(OAc)_6(py)_2pyr]^{n+}(PF_6)^-_n$ (n = 0, 1, 2) in CH_2Cl_2 for n = 0, 1 and in CH_3CN for n = 2, from 800 to 225 nm.

not carried sufficiently far to observe the 2+/1+ couple, and the 3+/2+ couple is beyond the solvent limit in acetone. They also failed to observe a reversible wave for the $[Ru_3O(OAc)_6(py)_3]^{0/1-}$ couple and instead reported an irreversible two-electron reduction past the +/0 wave. Our experience has been that in dry, deaerated acetonitrile both the 0/1− and 1−/2− couples are electrochemically reversible.

The most cathodic couple, $[Ru_3O(OAc)_6(L)_3]^{-/2-}$, appears to involve a localized ligand reduction (eq 1). The only real

$$[Ru_3O(OAc)_6(py)_2L]^- \xrightarrow{+e^-} [Ru_3O(OAc)_6(py)_2L]^{2-} \quad (1)$$

evidence for this conclusion is that the $E_{1/2}$ values follow the order of increasing ease of reduction of the free ligand ($E_{1/2}$ for the couples L + e → L⁻ in DMF vs. SSCE are at −2.08 for L = pyr, −1.87 for L = 4,4′-bpy, and L = −1.58 for BPE).[13] The influence of the nonpyridine ligand is also seen in the $[Ru_3O(OAc)_6(py)_2L]^{+/0}$ and $[Ru_3O(OAc)_6(py)L]^{0/1-}$ couples where the $E_{1/2}$ values are at slightly more positive potentials than the corresponding tris(pyridine) couples. The trend in potentials observed may follow the order of increasing back-bonding of the cluster to the ligand L: BPA < py < BPE = 4,4′-bpy < pyr. Consistent with this interpretation is the fact that the observed shifts are greater for the 0/1− couples where the electron content of the clusters is higher.

It is possible to prepare the 2+ clusters by controlled-potential electrolysis (Experimental Section). However, the 3+ clusters are only accessible on the cyclic voltammetry time scale. Attempted electrolyses past the 2+ → 3+ wave gave catalytic oxidation currents because of oxidation of solvent or possibly because of trace water in the solvent. Nonetheless, the cluster system remains intact following oxidation as shown by unchanged cyclic voltammograms following electrolysis.

Except for the relatively subtle effects found for the ligands, the $E_{1/2}$ observed values are essentially constant for the 2+/+, +/0, and 0/1− couples. The obvious exception is the CO cluster $[Ru_3O(OAc)_6(CO)(py)_2]$ where there are large positive shifts compared to the tris(pyridine) cluster. The carbonyl cluster will be discussed in more detail in a later section.

Optical Spectra. The clusters absorb light strongly in the near-ultraviolet and visible region, and the absorption extends into the very near-infrared for the neutral clusters. Optical spectra in the range 800–225 nm are shown in Figure 3 for the clusters $[Ru_3O(OAc)_6(py)_2pyr]^{n+}$ (n = 2, 1, 0) in CH_3CN for n = 2, CH_2Cl_2 for n = 1 and 0. The high light absorptivity in the visible is reminiscent of the oxo-bridged ions $[(bpy)_2ClRuORuCl(bpy)_2]^{2+}$,[7] $[A_5RuORuA_4ORuA_5]^{6+}$,[14] and $[Cl_5RuORuCl_5]^{4-}$,[15] where intense absorption bands can be assigned to transitions between molecular levels arising from $d\pi(Ru)$–$p(O)$ mixing.

Table II. Absorption Bands Obtained by Deconvolution of the Spectra of Clusters $[Ru_3O(OAc)_6(py)_2pyr]^{n+}$ (n = 0, 1, 2)

n = 0 (in CH_2Cl_2) λ_{max}, $cm^{-1} \times 10^3$ ($f \times 10^{-2}$)[a]	n = 1 (in CH_2Cl_2) λ_{max}, $cm^{-1} \times 10^3$ ($f \times 10^{-2}$)	n = 2 (in CH_3CN) λ_{max}, $cm^{-1} \times 10^3$ ($f \times 10^{-2}$)
		9.4 (0.59)
10.9 (16.0)	14.3 (6.49)	12.7 (5.29)
	16.6 (3.44)	17.4 (7.05)
18.3 (2.45)	19.6 (1.91)	22.4 (1.51)
21.2 (4.72)	26.0 (2.00)	26.6 (2.27)
24.3 (34.1)	30.6 (47.5)	32.2 (52.9)
34.0 (13.2)	35.5 (2.33)	34.6 (1.15)
39.8 (56.8)	41.3 (67.6)	38.3 (65.0)

[a] f = oscillator strength. Values were calculated using the spectral deconvolution program described above.

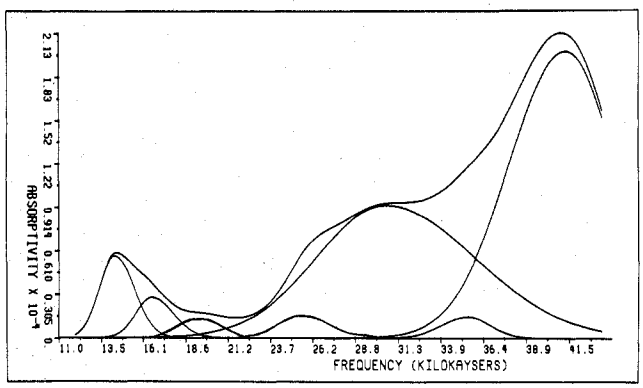

Figure 4. Results of spectral deconvolution of the electronic spectrum of $[Ru_3O(OAc)_6(py)_2pyr](PF_6)$ in CH_2Cl_2. The spectrum is linear in energy ($cm^{-1} \times 10^3$) with energy increasing from left to right which should be noted in making comparisons with Figure 5.

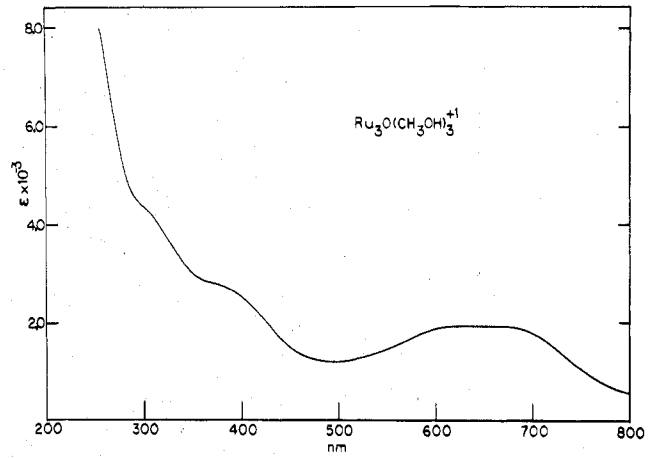

Figure 5. Ultraviolet–visible spectrum of $[Ru_3O(OAc)_6(CH_3OH)_3](OAc)$ in methanol from 800 to 240 nm.

The absorption bands are clearly composite bands and must originate from a series of closely spaced molecular electronic transitions. We have resolved several of the bands into their components using the program SPECSOLV.[11] In Table II are given in summary form the results of deconvolution studies on the series $[Ru_3O(OAc)_6(py)_2pyr]^{n+}$ (n = 0, 1, 2). The results of the deconvolution for the 1+ ion are shown graphically in Figure 4. In Table III are given in summary form λ_{max} values and extinction coefficients for the remaining clusters discussed here. In Table III no attempt has been made to summarize the appearance of shoulders and only the λ_{max} values for the most obvious features of the absorption envelopes are given.

In Figure 5 is shown the spectrum of the ion $[Ru_3O(OAc)_6(CH_3OH)_3]^+$ in methanol. The spectrum is shown because it is free of contributions to the observed spectra from

Table III. Ultraviolet-Visible Spectra in CH_2Cl_2

cluster	λ_{max}, nm (ϵ)	$cm^{-1} \times 10^3$
$[Ru_3O(OAc)_6(py)_2(CH_3OH)]^+$	685 (4420)	14.6
	693 (5230)	14.4
$[Ru_3O(OAc)_6(CO)(py)_2]$	585 (4590)	17.1
	345 (6570)	29.0
$[Ru_3O(OAc)_6(2\text{-Me(pyr)})_3]^{n+}$		
$n = 0$	900 (11400)[b]	11.1
	450 (16200)[b]	22.2
$n = 1$	693 (5940)	14.4
	360 (12000)	27.8
$[Ru_3O(OAc)_6(py)_3]^{n+}$		
$n = 0$	895 (6700)	11.2
	390 (11700)	25.6
	238 (22380)	42.0
$n = 1$	692 (5800)	14.5
	690 (5640)[a]	14.5
	240 (21000)	41.7
$n = 2$	775 (4300)[a]	12.9
	575 (3460)[a]	17.4
	312 (12600)[a]	32.1
	251 (19800)	39.8
$[Ru_3O(OAc)_6(py)_2pyr]^{n+}$		
$n = 0$	910 (10200)	11.0
	452 (8870)	23.2
	393 (9730)	25.5
	240 (25175)	41.7
$n = 1$	2200 (~110)	5.0
	692 (6200)	14.5
	243 (21800)	41.2
$n = 2$	775 (4530)	12.9
	575 (13570)	17.4
	313 (13400)	32.0
	256 (20500)	39.1
$[Ru_3O(OAc)_6(py)_2L]^+$		
L = 4,4'-bpy	694 (6400)	14.4
	244 (32580)	41.0
L = BPE	693 (6331)	14.4
	291 (32200)	34.4
L = BPA	692 (6100)	14.9
	242 (23800)	41.3

[a] In CH_3CN. [b] In benzene.

ligand-localized or cluster-ligand transitions involving the pyridine-type ligands. The spectrum of the tris(methanol) cluster in water where the cluster is almost surely the tris(aquo) cluster has the same absorption band pattern in both the low- and high-energy spectral regions. In clusters containing pyridine-type ligands, absorption in the ultraviolet is enhanced and distinct bands appear which are clearly assignable to $\pi^* \leftarrow \pi$ transitions localized on the pyridine-type ligands.

There are additional spectral differences in the high-energy region for the clusters which contain pyridine-type ligands. For example, the shapes of some of the spectral envelopes are different for the tris(pyridine) and bis(pyridine)–pyrazine clusters. It is most noticeable for the cluster $[Ru_3O(OAc)_6(py)_2pyr]^0$ where a distinct absorption maximum appears at 452 nm. The differences which appear in comparing the UV spectra for the 1+ and 2+ clusters suggest that either or both cluster-to-ligand or ligand-to-cluster charge-transfer transitions probably occur in this region.

Infrared Spectra. Much of the infrared spectra of the clusters from 2000 to 300 cm^{-1} are dominated by vibrational modes involving the bridging acetate groups. High-energy relatively weak ν(C–H) stretching bands are observed at ~2870 cm^{-1}. More intense asymmetric (1580 and ~1534 cm^{-1}) and symmetric (1417 cm^{-1}) carboxylate stretching frequencies occur at lower energies. The methyl groups of the acetates are represented by asymmetric (1447 cm^{-1}) and symmetric methyl bending modes (1346 cm^{-1}). Other bands apparently attributable to acetate modes occur at 941 and 677 cm^{-1}.

Pyridine-type ligands, where they are present, account for most of the remaining bands observed in the spectra. In the salt $[Ru_3O(OAc)_6(py)_3](PF_6)$, bands arising from the pyridines appear at 1610, 1489, 1219, 1160, 1071, 1047, 1015, 768, 692, 622, and 468 cm^{-1}. These can readily be assigned to the pyridine groups by comparison of the tris(pyridine) spectrum with the known spectrum of free pyridine.[16a] Two bands expected at about 1570 and 1440 cm^{-1} are apparently masked by carboxylate bands in the same region. In addition to the usual pyridine bands, the cluster salt $[Ru_3O(OAc)_6(py)_2pyr](PF_6)$ has two additional bands arising from the pyrazine ligand. One band overlaps with a carboxylate band at 1580 cm^{-1} (see below) and a second band appears at 1121 cm^{-1}.

In the carbonyl cluster $[Ru_3O(OAc)_6(CO)(py)_2]$, two carboxylate bands are observed in the asymmetrical stretching region at 1565 and 1599 cm^{-1}. Spencer and Wilkinson have argued that the appearance of two bands suggests a change from the symmetrical structure in Figure 1 to an asymmetrical structure in which there are four bridging and two bidentate carboxylate groups. However, the spectrum of the related cluster $[Ru_3O(OAc)_6(py)_2pyr]$ also includes an intense band at 1580 cm^{-1} which is absent in $[Ru_3O(OAc)(py)_3]^0$. The appearance of two bands in the asymmetric carboxylate stretching region may simply reflect a lowering of the molecular symmetry of the cluster rather than a change in primary structure. This interpretation is supported by ^1H NMR data as discussed in a later section.

The assignment of the band at 1580 cm^{-1} as a carboxylate band is somewhat complicated because it appears that a symmetric pyrazine stretching mode occurs at the same frequency. Evidence for the overlap of bands comes from the infrared spectrum of the symmetric pyrazine-bridged dimer $[(py)_2Ru_3O(OAc)_6(pyr)Ru_3O(OAc)_6(py)_2]$ which will be discussed in detail in a later paper. In the symmetric dimer, the symmetric pyrazine stretching mode is Raman active but infrared inactive. In the dimer, the second asymmetric carboxylate mode appears at 1590 cm^{-1} with roughly half the relative intensity of the band at 1580 cm^{-1} in $[Ru_3O(OAc)_6(py)_2pyr]$. Further, the cluster $[Ru_3O(OAc)_6(CH_3OH)_2CO]$[17] has the two asymmetric carboxylate modes at 1573 and 1613 cm^{-1} while $[Ru_3O(OAc)_6(pyr)_2CO]$[17] has both these bands as well as a distinct shoulder at about 1588 cm^{-1} which can be assigned to the symmetric pyrazine mode. It seems reasonable to conclude that there are overlapping carboxylate and pyrazine bands in both of the clusters $[Ru_3O(OAc)_6(py)_2pyr]^{+/0}$ but the relative intensity of the combined band appears to be diminished upon oxidation.

Other changes occur in band intensities with a change in cluster redox state. The pyridine stretch at 1601 cm^{-1} is enhanced in intensity upon oxidation of $[Ru_3O(OAc)_6(py)_3]$ to $[Ru_3O(OAc)_6(py)_3]^+$ while a second pyridine stretch at 1479 cm^{-1} is noticeably weakened. Similar changes in intensity on oxidation are seen for several other bands, both ring and proton modes. The changes suggest that a coupling exists between certain modes and that the coupling is influenced by the electron content of the cluster. The same effect is observed for the clusters $[Ru_3O(OAc)_6(py)_2(pyr)]^{+/0}$.

ESCA. Ru $3d_{5/2}$ binding energy data are given in Table IV for the clusters $[Ru_3O(OAc)_6(py)_3](PF_6)_n$ (n = 0, 1, 2) and for some other ruthenium complexes which are useful for purposes of comparison. The expected $3d_{3/2}$ bands are masked by the large C 1s band at 284.4 eV. The $3d_{5/2}$ binding energies in Table IV are relative to the C 1s peak at 284.4 eV.

The binding energy data are remarkable for two reasons. The neutral and 2+ clusters are mixed-valence cases, where, assuming localized valences, the oxidation states at Ru are for $[Ru_3O(OAc)_6(py)_3]^0$ (2, 3, 3) and for $[Ru_3O(OAc)_6(py)_3]^{2+}$

Table IV. Ru $3d_{5/2}$ ESCA Data for the Clusters $[Ru_3O(OAc)_6(py)_3](PF_6)_n$ (n = 0, 1, 2) and Related Compounds

compound	formal oxidation states[a]	binding energy,[b] eV
$[Ru_3O(OAc)_6(py)_3]$	3, 3, 2	279.3
$[Ru_3O(OAc)_6(py)_3](PF_6)$	3, 3, 3	280.4
$[Ru_3O(OAc)_6(py)_3](PF_6)_2$	3, 3, 4	281.0
$[(bpy)_2ClRuORuCl(bpy)_2](PF_6)_2$	3, 3	280.5[c]
$[(bpy)_2ClRuORuCl(bpy)_2](PF_6)_3$	3, 4	282.3[c]
$[Ru(bpy)_2Cl_2]$	2	279.9[d]
$[Ru(bpy)_2Cl_2]Cl$	3	281.9[d]
$[Ru(NH_3)_6]I_2$	2	280.2[d]
$[Ru(NH_3)_6](PF_6)_3$	3	282.6[d]

[a] Assuming localized valences. [b] The binding energy of C 1s is taken as 284.4 eV. [c] Reference 7. [d] E. C. Johnson, Ph.D. Dissertation, The University of North Carolina, Chapel Hill, 1975, Chapter 5.

(3, 3, 4). However, for all three clusters, only a single binding energy is observed. This is, of course, expected for $[Ru_3O(OAc)_6(py)_3]^+$ where the formal oxidation states are the same (3, 3, 3). For the other two it suggests that the Ru sites are equivalent and the clusters delocalized on the ESCA time scale. In fact, given the observation of a single Ru $3d_{5/2}$ band and the recent work of Hush,[18] it appears that the Ru sites are *strongly* coupled in both of the mixed-valence clusters. There is also a surprisingly slight shift in binding energy upon oxidation of the 0 cluster to the +1 and +2 clusters. As shown in Table IV for a series of Ru(II) and Ru(III) salts, the $3d_{5/2}$ binding energies measured using the same spectrometer and some conditions gave values of 279.9–280.2 eV for a series of Ru(II) complexes and 281.9–282.6 eV for a series of Ru(III) complexes. The binding energy for the neutral cluster is that for Ru(II) and loss of two electrons moves it into the binding energy range expected for Ru(III). A similar but less dramatic effect is observed for the oxo-bridged dimers[7] $[(bpy)_2ClRuORuCl(bpy)_2]^{m+}$ (m = 2, 3). A single binding energy is observed for the mixed-valence (3, 4) 3+ ion in the range expected for Ru(III) and the binding energy for the 2+ (3, 3) ion is nearer that expected for Ru(II) than for Ru(III). In both the dimeric and trimeric systems, the binding energy shifts relative to monomeric Ru(II) and Ru(III) complexes probably reflect the effects of delocalization arising from extensive orbital overlap between sites. The extent of the effect appears to be greater in the trimeric clusters.

^{1}H Nuclear Magnetic Resonance. The ^{1}H NMR spectra of the complexes $[Ru_3O(OAc)_6(py)_3]$, $[Ru_3O(OAc)_6(py)_3](PF_6)$, $[Ru_3O(OAc)_6(py)_2pyr]$, and $[Ru_3O(OAc)_6(py)_2pyr](PF_6)$ were obtained in CD_2Cl_2, since all complexes have an appreciable solubility in dichloromethane. The observed chemical shifts were measured relative to Me_4Si at δ 0 and are accurate to ±0.02. The results are summarized in Table V. Delta values (Δ) are the magnitudes of the chemical shift changes in parts per million which occurred upon oxidation of the diamagnetic 0 cluster to the paramagnetic +1 cluster. A similar experiment was reported by Spencer and Wilkinson for the tris(pyridine) clusters in benzene, but their data did not distinguish between the ortho, meta, and para resonances of the pyridine ligands and peak integrations were not reported. The data are of interest for two reasons. First relatively small paramagnetic shifts are observed for the paramagnetic clusters and the line widths are not appreciably broadened compared to the neutral clusters. Second, the methyl resonances of the acetate groups, which occur at the same chemical shift for the tris(pyridine) clusters, are split into two distinct types in the bis(pyridine)pyrazine clusters. The splitting is especially noticeable for the 1+ cluster. The observation of a similar splitting in the acetate resonances for $[Ru_3O(OAc)_6(py)_2CO]$ was interpreted by Spencer and Wilkinson as supporting evidence for the change in cluster structure alluded to above. However, IR and ^{1}H NMR comparisons with the clusters $[Ru_3O(OAc)_6(py)_2pyr]^{+/0}$ suggest that the spectral changes observed can be explained by a lowering in the molecular symmetry rather than by a change in structure.

Table V. ^{1}H NMR Chemical Shift Data for the Paramagnetic 1+ and Diamagnetic 0 Clusters $[Ru_3O(OAc)_6(py)_2]^{n+}$ (n = 0, 1+) in CD_2Cl_2 Relative to Me_4Si at δ 0

	$[Ru_3O(OAc)_6(py)_3]^0$		$[Ru_3O(OAc)_6(py)_3]^+$		
L = py	δ	(n)[a]	δ	(n)[a]	Δ[b]
C-H pyridine, ortho	9.02	(6.0)	0.45	(5.2)	8.57
meta	7.69	(6.1)	5.76	(6.0)	1.93
para	7.99	(3.2)	6.51	(2.4)	1.48
C-H acetate	2.14	(17.8)	4.83	(18.0)	−2.69
	$[Ru_3O(OAc)_6(py)_2pyr]^0$		$[Ru_3O(OAc)_6(py)_2pyr]^+$		
L = pyr	δ	(n)[a]	δ	(n)[a]	Δ[b]
C-H pyridine, ortho	9.30	(4.0)	−0.50	(3.4)	9.80
meta	7.79	(4.2)	4.83	(4.0)[e]	2.96
para	8.03	(1.9)	5.81	(2.0)	2.22
C-H pyrazine, ortho	8.79	(2.0)	0.7	(2.0)	8.09
meta	9.06	(2.2)	5.52	(2.1)	3.54
C-H acetate, cis[c]	2.09	(12.0)[d]	4.34	(11.8)	−2.25
trans[c]	2.04	(6.0)[d]	4.82	(6.0)[e]	−2.78

[a] Relative number of protons by integration. [b] Δ(the contact shift values) = $\delta(0) - \delta(1)$ for each of the different chemical sites. [c] Cis and trans relative to the pyr ligand. [d] Peaks overlap, total integration = 18. [e] Peaks overlap, total integration = 10.

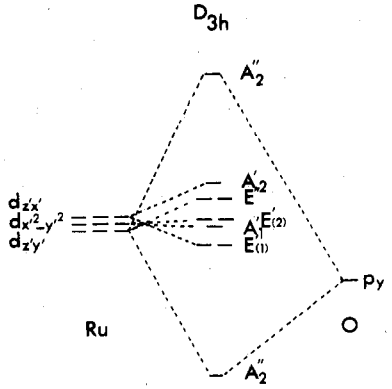

Figure 6. Qualitative molecular orbital scheme for the cluster π system in D_{3h} symmetry.

Discussion

The overall structure of the ruthenium–μ-oxo cluster system shown in Figure 1 is based on the crystallographic results of Cotton and Norman[2] for the compound $[Ru_3O(OAc)_6(PPh_3)_3]^0$. Cotton and Norman also proposed a qualitative molecular orbital scheme for the cluster π-electronic system. A more detailed diagram based on their original scheme is shown in Figure 6. In the diagram the central oxygen atom is considered to be sp^2 hybridized in order to account for the Ru_3O σ-bonding framework. This leaves a single p orbital of π-type symmetry on the oxygen atom. The orbital combinations used to construct the diagram are based on a coordinate axis system at each ruthenium site as shown in Figure 7. The axis system and orbitals chosen are convenient because they emphasize pictorially the probable importance of Ru–O–Ru mixing.

The molecular orbitals chosen do not lie along the coordinate axes of the individual ruthenium sites. In the axis system used, molecular orbitals can be constructed by d_{zy}–p_{0z} combinations. In the D_{3h} symmetry of a symmetrical $[Ru_3O(OAc)_6(L)_3]$ cluster unit, the d_{zy}–p_{0z} combinations give rise to the two A_2''

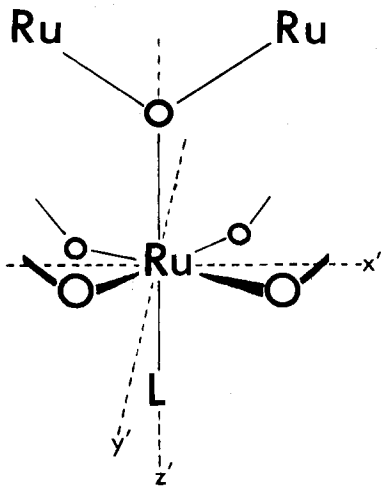

Figure 7. Local coordinate system for the individual ruthenium sites. Z' and X' lie in the Ru_3O plane and Y' is perpendicular to the plane.

levels in the diagram and $d_{zy'}$–$d_{zy'}$ combinations to the E″ level. According to the scheme and the relative energies of the atomic orbitals involved, the lowest A_2'' level should be largely oxygen in character, the E″ level a degenerate pair which is nonbonding, and the highest A_2'' level should be largely Ru in character and antibonding.

Direct Ru–Ru combinations can be constructed by mixing $d_{x'z}$–$d_{x'z}$ orbitals based on the three Ru sites. The orbitals are directed at each other and their combination in the D_{3h} symmetry of the cluster gives rise to degenerate, metal–metal bonding, E′(1), and the nondegenerate antibonding, A_2', levels shown in the diagram. The three M–M based orbitals are in the same plane as the in-plane sp^2 hybrids on the central oxygen which for purposes of the scheme are assumed to be involved only in the Ru–O–Ru σ-bonding framework. The choice of A_2' (M–M antibonding) at higher energy than E″ (M–O–M nonbonding) is somewhat arbitrary but is reasonable given the spectral data to be discussed below.

The remaining $d\pi$ orbitals ($d_{x'^2-y'^2}$) are of appropriate symmetry to interact via a through-space interaction but are separated by a considerable distance. These same orbitals can also interact by symmetry with p orbitals localized on the oxygen atoms of the bridging acetates, which would provide a further mechanism for Ru–Ru interaction. Given the relative distances involved, we assume that the latter mechanism for Ru–Ru interaction is relatively unimportant compared to the Ru–O–Ru and direct Ru–Ru interactions. However, we have assumed that the interaction is sufficient to remove the degeneracy of the three $d_{x'^2-y'^2}$ orbitals and this is the origin of the degenerate pair, E′(2) and the singlet A_1' in the scheme. Mixing of the $d_{x'z}$ and $d_{zy'}$ orbitals with acetate oxygen p orbitals can also occur but the effect of such mixing is assumed to be small and was neglected in constructing the diagram.

Both the pyridine and pyrazine ligands have π and π^* orbitals which have symmetries appropriate for overlap with ruthenium d orbitals at the three Ru sites. If the plane of the ligand is parallel to the plane of the cluster, ligand π and/or π^* interactions could occur with the delocalized A_2'' or E″ orbitals. If the ligand plane is perpendicular to the cluster plane, interactions could occur with A_2' or E′. Since the ligands are probably freely rotating in solution at room temperature, all four orbitals will be somewhat affected. Interactions with the ligand π or π^* orbitals are not included in the diagram explicitly.

The schematic energy level diagram presented is consistent with the observed chemical and physical properties of the clusters. The highest occupied levels are either A_2' or E″, which are only partly occupied in the paramagnetic cluster $[Ru_3O(OAc)_6(L)_3]^+$. The influence of the unpaired electron in the 1+ cluster is seen in the paramagnetic shifts in its ^1H NMR spectrum compared to the spectrum of the neutral cluster. Resonances are observed for both $-CH_3$(acetate) and pyridine protons (Table V). Only slight paramagnetic shifts occur in the 1+ cluster and the line widths are not noticeably broadened. There is no evidence for selective paramagnetic shifts for the ortho, meta, or para C–H positions of the pyridine ligands since resonance envelopes for all three positions are shifted to higher fields. The results are consistent with an interpretation where the paramagnetic shifts of the ring protons arise largely from pseudocontact, through space magnetic interactions between the ligands and unpaired spin density localized within the Ru–O–Ru cluster framework. From the scheme in Figure 6, the unpaired electron is in either the A_2' or E″ levels which can interact by symmetry with the π or π^* pyridine levels. The absence of noticeable Fermi contact shifts from the ^1H NMR data and the absence of obvious cluster → pyridine or pyridine → cluster charge-transfer bands both suggest that π or π^*(pyridine) interactions with the metal sites in the 1+ cluster are small. The opposite sense of the shifts for the acetate methyl and pyridine protons must arise because of the different geometrical positions of the two types of ligands relative to the spatial character of the unpaired electron density.

From the electronic spectral data obtained by deconvolution, the lowest energy visible absorption band actually consists of three well-defined components for the 0, 1+, and 2+ clusters (Figures 4 and 5 and Tables II and III). The results of the deconvolutions are reasonable since distinct shoulders are evident at appropriate wavelengths in the actual spectra (compare Figures 4 and 5). From the scheme in Figure 8 the origins of the two low-energy components at 1.43 and 1.66 μm^{-1} for the cluster $[Ru_3O(OAc)_6(py)_2pyr]^+$ are consistent with the intracluster transitions $A_2'' \leftarrow E''$ and $A_2'' \leftarrow A_1'$, both of which are symmetry allowed. The third component for the 1+ cluster at 1.96 μm^{-1} is noticeably weaker in intensity and its origin is consistent with the transition $A_2'' \leftarrow E'(1)$ which is not electric dipole allowed in D_{3h} symmetry but is in C_{2v} symmetry. The origin of its intensity in D_{3h} clusters like the tris(pyridine) 1+ cluster may come from slight molecular distortions. The transition $A_2'' \leftarrow A_2'$ is not allowed in either D_{3h} or C_{2v} symmetry.

Essentially the same pattern of low-energy absorption bands is observed for all three cluster types 0, 1+, 2+, but the transition energies do respond to changes in the electronic content of the cluster. In comparing $[Ru_3O(OAc)_6(py_3]^{2+}$ to $[Ru_3O(OAc)_6(py)_3]^+$, the two higher energy transitions are blue shifted and the low-energy transition is red shifted. The blue shifts for the $A_2'' \leftarrow E'(1)$ and $A_2'' \leftarrow A_1'$ transitions suggest that loss of an electron must stabilize the donor metal–metal bonding E′(1) and Ru-localized (essentially nonbonding) A_1' levels more than the acceptor Ru–O–Ru antibonding level (A_2''). The red-shifted band corresponds to the $A_2'' \leftarrow E''$ transition which involves electronic excitation to the A_2'' Ru–O–Ru antibonding level from the nonbonding E″ levels. The decrease in energy for this transition suggests that the energy of the E″ level is even less affected by oxidation to the 2+ cluster than is the A_2'' level.

For the neutral cluster $[Ru_3O(OAc)_6(py)_2pyr]^0$ all three components of the low-energy absorption envelope are red shifted. The shifts to lower energy are consistent with a general destabilization of the occupied E″, E′(1), and A_1' levels arising from increased electron–electron repulsion.

If the assignments for the visible absorption bands are correct, an estimate of the relative energies of the A_2' and E″ levels can be obtained. From the difference in energies for the transitions $A_2'' \leftarrow A_1'$ (1.66 μm^{-1}) and $A_2'' \leftarrow E''$ (1.43

μm^{-1}), the E″ (M–O–M nonbonding) orbital is destabilized by about 0.23 μm^{-1} relative to the nonbonding A_1' level in $[Ru_3O(OAc)_6(py)_2pyr]^+$. Comparing the energies for the transitions $A_2'' \leftarrow E'(1)$ (M–M bonding) (1.96 μm^{-1}) and $A_2'' \leftarrow A_1'$ (1.66 μm^{-1}) shows that the E′(1) (M–M bonding) level is stabilized by about 0.30 μm^{-1} relative to the A_1' level. The antibonding metal–metal complement to the degenerate pair E′(1) is A_2'. A_2' then ought to be destabilized by twice as much as the E′(1) level is stabilized. The amount of destabilization is 0.60 μm^{-1} relative to A_1' compared to 0.23 μm^{-1} for E″ relative to A_1'. This argument is the basis for choosing A_2'' to be of higher energy than E″ in the MO diagram.

Realistically, the changes in optical spectra with changes in cluster electronic content are remarkably small and suggest that electrons must be gained or lost from extensively delocalized molecular orbitals. The spectral results are consistent with the results of the Ru $3d_{5/2}$ ESCA experiment where only a single binding energy is observed for the mixed-valence clusters $[Ru_3O(OAc)_6(py)_3]^n$ (n = 0 or 2+) and only small shifts in binding energy are observed as the electron content of the cluster is changed.

In the optical spectra, additional multiple-component absorption bands appear at higher energies. The multiple transition nature of the absorption envelopes is indicated by the appearance of distinct shoulders. The bands alluded to are in addition to the $\pi^* \leftarrow \pi$(pyridine) bands which were mentioned earlier. There are several possibilities for the origins of the higher energy bands. One of the more interesting possibilities is that given the spread in energies between delocalized cluster levels, it is possible that *both* ligand-to-cluster (A''_2 (antibonding Ru–O–Ru) $\leftarrow \pi$(py)) and cluster-to-ligand (π^*(py) $\leftarrow A''_2$, etc.) charge-transfer bands may appear in this spectral region for certain of the clusters.

In addition to the higher energy bands, bands appear for the clusters at very low energies. In the 2+ cluster $[Ru_3O(OAc)_6(py)_2pyr]^{2+}$, the results of the spectral deconvolution studies show that a weak, low-energy band appears at 0.99 μm^{-1}. For the 1+ cluster $[Ru_3O(OAc)_6(py)_2pyr]^+$ a weak band appears in the near-infrared. λ_{max} for the band was not determined because it was still increasing in intensity at the solvent cutoff (2200 nm). Spectral measurements at lower energies were not possible because of strong solvent absorptions. The low-energy bands may involve transitions between cluster levels which are essentially d(Ru) in character. They would involve excitations from lower energy d-Ru levels to the holes in the vacant (in $[Ru_3O(OAc)_6(py)_2pyr]^{2+}$) or half-filled (in $[Ru_3O(OAc)_6(py)_2pyr]^+$) A_2' level (e.g., $A_2' \leftarrow E'(1)$). In the 1+ tris(aquo) and tris(methanol) clusters, similar low-energy bands appear but at slightly higher energies (1.19 and 1.16 μm^{-1}). The bands are noticeably more intense for these two ions.

$[Ru_3O(OAc)_6(CO)(py)_2]$. On the basis of infrared and NMR evidence and the fact that the cluster undergoes an unsymmetrical splitting reaction with PPh_3 to give the dimer $[Ru_2O(OAc)_3(CO)(PPh_3)]$, Spencer and Wilkinson[1b] proposed that the carbonyl–dipyridinate cluster has the unsymmetrical structure shown. From our work, it appears that the basic

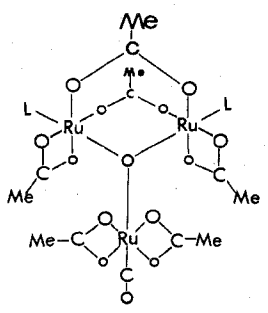

cluster molecular structure is maintained in $[Ru_3O(OAc)_6(CO)(py)_2]$ but that the effect of the bound CO on the *electronic* structure of the cluster system is profound.

The IR evidence discussed earlier suggests that the origin of the two asymmetric carboxylate stretching modes may simply be from a lowering of the symmetry of the cluster. The appearance of two methyl resonances in the ^1H NMR spectrum may have the same origin. Other evidence of a chemical nature suggests that the molecular structure remains unchanged in the CO cluster. It is prepared from symmetrical clusters by simple displacement reactions under mild conditions (eq 2). It undergoes two reversible one-electron oxidations

$$[Ru_3O(OAc)_6(py)_2L] + CO \rightarrow [Ru_3O(OAc)_6(py)_2CO] \quad L = \text{py or solvent} \qquad (2)$$

on the cyclic voltammetry time scale. The first oxidation is followed by slower loss of CO to give the clusters $[Ru_3O(OAc)_6(py)_2S]^+$ where S is CH_3OH or CH_3CN where again the basic cluster structure is maintained as shown by their redox and spectral properties.

The structural integrity of the cluster unit may be maintained, but the presence of the CO group has a profound effect on the properties of the cluster. $E_{1/2}$ values for the $0 \rightarrow 1+$ and $1+ \rightarrow 2+$ oxidations are shifted to significantly higher potentials (by ~670 and 290 mV) compared to the tris(pyridine) cluster (Table I). The optical spectrum is considerably changed and the remarkably consistent pattern of cluster electronic transitions is no longer observed in the carbonyl cluster (Table III).

The major effect of the CO group is probably exerted through back-bonding from Ru to CO. Back-bonding must influence the Ru sites bound to CO rather strongly and through it the electronic properties of the cluster π-electronic system. Since CO is bound to a single Ru site, the symmetrical electronic structure assumed in the qualitative MO treatment in Figure 6 is no longer appropriate. In the CO cluster there is no doubt an extensive electronic asymmetry with two sets of nearly localized levels, one based on the Ru–CO site and the other on the remaining dimeric Ru–O–Ru unit.

In a general way, $d\pi$–π^*(CO) back-bonding removes electron density from the cluster π-redox orbitals which leads to the higher potentials for cluster oxidation. The importance of back-bonding in determining the stability of the Ru–CO bond can be seen in the 1+ cluster $[Ru_3O(OAc)_6(py)_2CO]^+$ where the π-electron content has been lowered and the CO group labilized toward substitution.

Conclusions

The oxo-bridged, triruthenium acetate clusters are remarkable for their extensive multiple redox properties. Their redox and spectral properties appear to be understandable in terms of a delocalized, cluster-based π-molecular orbital system where the redox levels are largely Ru–Ru and Ru–O–Ru in character. As shown by chemical isolation and spectral studies, the equivalent nature of the Ru sites is maintained in at least the 0, 1+, and 2+ clusters. Interconversions between the redox states $[Ru_3O(OAc)_6(L)_3]^{3+/2+/+/0/-}$ involve changes in electron population in Ru–Ru metal–metal bonding and Ru–O–Ru nonbonding and antibonding molecular levels. Assuming that the pattern of levels in Figure 6 remains the same in the various redox states, one-electron oxidations of the neutral cluster $[Ru_3O(OAc)_6(L)_3]$ involve stepwise loss of electrons first from A_2' (metal–metal antibonding) to give the 1+ and 2+ clusters. Loss of a third electron to give the transient 3+ cluster occurs from the degenerate Ru–O–Ru nonbonding E″ levels. Reduction of the neutral cluster occurs first at the vacant Ru–O–Ru antibonding level A_2'', apparently followed by a ligand π^*-based reduction. If this interpretation is correct,

the doubly reduced 2- cluster could have most interesting magnetic and low-energy electronic absorption spectral properties.

Changes in the terminal ligands on the periphery of the cluster such as exchanging pyridines for methanol or going from symmetrical, $[Ru_3O(OAc)_6(py)_3]^{n+}$, to unsymmetrical, $[Ru_3O(OAc)_6(py)_2pyr]^{n+}$, clusters lead to relatively slight but understandable changes in cluster properties. However, in the neutral carbonyl cluster $[Ru_3O(OAc)_6(py)_2CO]$, the single CO group creates a large electronic asymmetry and the properties of the CO cluster are significantly modified. The importance of Ru → CO back-bonding is seen in the lability of the CO group following oxidation to the 1+ cluster, a reaction which can be exploited synthetically to give unsymmetrically substituted clusters and, ultimately, dimers and higher oligomers. Because of the effect of the CO group, the electronic structure and chemical properties of this cluster may be understandable in terms of interacting but reasonably localized Ru–CO and Ru–O–Ru dimeric sites.

Acknowledgment. Acknowledgments are made to the Army Research Office–Durham under Grant No. DAAG29-76-G-0135 and to the donors of the Petroleum Research Fund, administered by the American Chemical Society, for support of this research. The authors wish to express their appreciation for the contributions of Pamela L. Hood and for her efforts in the completion of the work.

Registry No. **1**, 67815-37-6; **2**, 67815-38-7; **3**, 37337-93-2; **4**, 52933-80-9; **5**, 67815-39-8; **6a**, 67815-40-1; **6b**, 67815-42-3; **6c**, 67815-44-5; **6d**, 67815-46-7; **7**, 67951-63-7; **8a**, 67921-62-4; **8b**, 68024-67-9; **9**, 67951-61-5; **10**, 67815-48-9.

References and Notes

(1) (a) A. Spencer and G. Wilkinson, *J. Chem. Soc., Dalton Trans.*, 1570 (1972); (b) *ibid.*, 786 (1974).
(2) F. A. Cotton and J. G. Norman, Jr., *Inorg. Chim. Acta*, **6**, 411 (1972).
(3) T. J. Meyer, *Ann. N.Y. Acad. Sci.*, in press.
(4) T. J. Meyer, *Acc. Chem. Res.*, **11**, 94 (1978).
(5) T. J. Meyer, *Adv Chem. Ser.*, No. **150**, Chapter 7 (1976).
(6) R. W. Callahan, E. C. Johnson, G. M. Brown, T. R. Weaver, and T. J. Meyer, *ACS Symp. Ser.*, No. **5**, 66 (1975).
(7) T. R. Weaver, S. A. Adeyemi, G. M. Brown, R. P. Eckberg, W. E. Hatfield, E. C. Johnson, R. W. Murray, D. Untereker, and T. J. Meyer, *J. Am. Chem. Soc.*, **97**, 3039 (1975).
(8) R. W. Callahan and T. J. Meyer, *Chem. Phys. Lett.*, **39**, 82 (1976); R. W. Callahan, F. R. Keene, D. J. Salmon, and T. J. Meyer, *J. Am. Chem. Soc.*, **99**, 1064 (1977).
(9) M. J. Powers, D. J. Salmon, R. W. Callahan, and T. J. Meyer, *J. Am. Chem. Soc.*, **98**, 6731 (1976).
(10) S. T. Wilson, R. F. Bondurant, T. J. Meyer, and D. J. Salmon, *J. Am. Chem. Soc.*, **97**, 2285 (1975).
(11) (a) H. Gold, C. E. Rechsteiner, and R. P. Buck, *Anal. Chem.*, **48**, 1540 (1976); (b) H. S. Gold, "SPECSOLV-A Generalized Spectral Deconvolution Program", Library Science Series Document LS-301, Research Triangle Park, Triangle Universities Computation Center, 1976.
(12) (a) R. G. Cavell, W. Byers, and E. D. Day, *Inorg. Chem.*, **10**, 2710 (1971). (b) An examination and discussion of curve resolution techniques appears in H. A. Kuska, D. H. Beebe, and F. L. Urbach, *Anal. Chem.*, **46**, 2220 (1974).
(13) (a) K. B. Wiberg and T. P. Lewis, *J. Am. Chem. Soc.*, **92**, 7154 (1970); (b) J. Volke and J. Holubek, *Collect. Czech. Chem. Commun.*, **27**, 1777 (1962).
(14) J. E. Early and T. Fealey, *Inorg. Chem.*, **12**, 323 (1973).
(15) (a) J. D. Dunitz and L. E. Orgel, *J. Chem. Soc.*, 2594 (1953); (b) J. S. Filippo, Jr., P. J. Fagan, and F. J. DiSalvo, *Inorg. Chem.*, **16**, 1017 (1977); (c) R. J. H. Clark, M. L. Franks, and P. O. Turtle, *J. Am. Chem. Soc.*, **99**, 2473 (1977).
(16) (a) L. Corrsin, B. J. Fax, and R. C. Lord, *J. Chem. Phys.*, **21**, 1770 (1953); (b) R. C. Lord, A. L. Marston, and F. A. Miller, *Spectrochim. Acta*, **9**, 113 (1957).
(17) Details concerning the preparation and properties of this cluster will appear in a later publication.
(18) N. S. Hush, *Chem. Phys.*, **10**, 361 (1975).

Contribution from the Departments of Chemistry, Georgetown University, Washington, D.C. 20057, and George Mason University, Fairfax, Virginia 22030

Linear Free Energy Relationship for Outer-Sphere Reduction of Ruthenium(III) Amine Complexes by Titanium(III)

KEITH M. DAVIES and JOSEPH E. EARLEY*

Received April 17, 1978

Second-order rate constants k have been measured for reactions by which various Ru(III) complexes are reduced to corresponding Ru(II) complexes by $TiOH^{2+}$. At 25 °C, in media of 1 M ionic strength, values of k (M^{-1} s^{-1}) are as follows: $Ru(NH_3)_5H_2O^{3+}$, 66; $Ru(NH_3)_5py^{3+}$, 4.2×10^3; $Ru(NH_3)_5pyr^{3+}$ (pyr = pyrazine), 1.5×10^5; *cis*-$Ru(NH_3)_4(isn)_2^{3+}$ (isn = isonicotinamide), 1×10^6. For the last-named complex, a path involving reduction by Ti^{3+} ($k^\circ = 2 \times 10^4$ M^{-1} s^{-1}) was also observed. The values of k are found to follow a linear free energy relationship with slope near $^1/_2$, when plotted against the reduction potentials of the Ru(III) complexes. The variation in rate constant with $\mathcal{E}^\circ$ is mainly due to a variation in enthalpy of activation.

Introduction

Rates of redox reactions of inorganic ions are often sensitive to variation in thermodynamic driving force. Even before mechanistic and theoretical understanding was well developed, it had been shown that certain redox systems followed linear free energy relationships (LGR); that is, straight lines were obtained when log k was plotted against ΔG°.[1] Sutin,[2] and later other workers, demonstrated that a number of sets of reactions involving the outer-sphere electron-transfer mechanism follow LGR. We have also shown[3] that Cr(II)–Cr(III) electron-transfer reactions (which involve the inner-sphere mechanism) follow a LGR with a slope near $^1/_2$. When free-energy data are not available, "indirect" LGR (involving either or both mechanisms) can sometimes be obtained by comparing rates of reduction of various reductants with a series of common oxidants.[4]

Chow, Creutz, and Sutin[5] have called attention to a number of factors which could complicate interpretation of rates of electron-transfer reactions in terms of theory. One such factor is variation in the extent of electron-donor orbital, electron-acceptor orbital interaction in the transition state. Since both of these orbitals have t_{2g} symmetry for Ru(III)–Ti(III) reactions, such overlap is favored. This effect has previously[6a] been invoked to explain one of the chemical peculiarities which is common to Ru(II) and Ti(III), that is, facile reduction of ClO_4^- ion. The present paper deals with simple outer-sphere

* To whom correspondence should be addressed at Georgetown University.

0020-1669/78/1317-3350$01.00/0